# Note on the stability of the lattice Boltzmann phase propagation equation for the binary-liquid model

A. KUZMIN
*Chemical Engineering Department, University of Alberta*
*Edmonton, Alberta, Canada*
*shurik.kuzmin@gmail.com*

I. GINZBURG
*Irstea*
*Antony, France*
*irina.ginzburg@irstea.fr*

During recent years the binary-liquid Lattice Boltzmann model (LBM) has been applied for a wide range of applications, including the spinoidal decomposition [35, 45], capillary fillings [48] and contact angle measurements [4, 47] . However, its applicability for practical problems remains limited due to its still undetermined stable parameter space. The modelled binary liquid system is described by the two-phase Navier-Stokes equation coupled with the phase propagation equation for interface motion, based on the non-linear chemical potential relationship. In the past, the hydrodynamic LBM schemes have been extended for flow field modeling, while the advection-diffusion schemes with the non-linear equilibrium function apply for solving phase propagation equation. In addition to relaxation parameters of the involved LBM scheme, and flow field velocity $U$, their equilibrium parameter space includes two additional coefficients: $k$ and $A$ used for chemical potential, along with the interface mobility coefficient $\Gamma$. This work develops a stability study of the complex interplay in parameter space $(A, k, \Gamma, U)$, versus relaxation rates, and with a focus on the modelling of small capillary numbers for large lattice velocities.

We present von Neumann stability analysis for the linearized phase propagation equation modelled by single-relaxation-time (BGK) one-dimensional (D1Q3) scheme. The exact (in diffusion limit) and semi-analytical (advection-diffusion) results follow, respectively, the necessary and sufficient conditions predicted for linear schemes [29]. In particular, they respect the intrinsic relations between the stability curves and the non-negativity of equilibrium distributions. However, numerical simulations reveal that with the increase of the velocity, the predicted parameter map is only valid when the BGK relaxation rate $w$ lies far enough from its linear stability limit $w = 2$, where the diffusion coefficient vanishes. On the other hand, replacing the BGK operator by the optimal two-relaxation-times (TRT) collision operator [29], the numerical simulations match closely TRT stability predictions. They confirm that the optimal TRT collision offers larger stable areas, which are independent of diffusion relaxation values. Thus, the presented analysis contributes to fill a gap between the linear stability results and non-linear simulations. We believe that our simple numerical recipes for a proper choice of relaxation rates and two-phase parameter relationships are valuable for academic and practical simulations.

*Keywords*: Lattice Boltzmann Method; Binary-liquid model; Stability of the phase equa-

tion; BGK/TRT collision operator, von Neumann stability analysis

PACS Nos.: 47.11.-j, 47.55.-t, 02.60.-x

## 1. Introduction

Since two last decades, originated from the lattice gas automata for hydrodynamics problems [16, 32, 33], the lattice Boltzmann method became a powerful CFD competitor, with the ability to simulate from micro flows to thermal flows [67], ferrofluids [8] and other fluids with complex rheological behavior [26, 63], shallow water [7, 46] and macroscopic variably saturated flows [20, 31]. The associated multi-component transport of contaminants in porous packings [43, 66], mesoscale flows [14, 64] and large aquifers [5, 42, 54] is modeled via linear and highly nonlinear advection-diffusion LBE schemes. This method offers indisputable advantages for modeling in porous structures [15, 59] and for complex interface phenomena [1, 2, 26, 30, 60], because of its intrinsic possibility to correctly mimic the underlying physical behaviour via simple and often intuitive modifications of the population update on the boundaries and interfaces. Well known examples of that are the bounce-back and specular reflexion boundary rules, or the "recoloring", anti-diffusion algorithm for immiscible fluids, [30]. A thorough review on two phase models and the derivation of their governing macroscopic equations can be found in the recent work [62].

Associated numerical analysis aims at improving the accuracy of the method for arbitrary shaped boundaries, [3, 6, 19, 25, 27], interface description [12, 18, 21, 34, 41, 51, 61] or consistency of truncation corrections with respect to physical model [13, 40]. Also, in different degrees, all the LBE two-phase models suffer from typical numerical artifacts, like spurious currents associated with the interface [17, 18, 56, 62]. A more involved treatment of the multiphase interaction in free energy model [36, 58] and the Shan-Chen model [57] solves the problem partly and also shows some stability improvement. This last point is crucial for industrial applications of the method.

In fact, every practical problem requires to cover a specific parameter range in terms of the dimensionless numbers, as Reynolds, Froude or Péclet. In case of the two-phase hydrodynamics, additionally, the capillary number ($Ca$), viscosity and density ratios, as $\frac{\nu_{liq}}{\nu_{gas}}$ and $\frac{\rho_{liq}}{\rho_{gas}}$, should be respected. The problem is how to match all of them within the available degrees of freedom of the LBE scheme, such as: on the one hand, the equilibrium parameters, typically: velocity, diffusion or surface tension scalings; and, on the other hand, the relaxation rates of the collision operator. Moreover, some equilibrium terms can adapt different underlying discretization stencils by simple modification of their free-tunable weights. A very specific feature of the multiple-relaxation-times LBE (MRT) models [9, 11, 32, 33] and two-relaxation-times (TRT) scheme [21] for hydrodynamics and transport is that one (TRT) or several (MRT) relaxation rates are also free-tunable. Their simplest common subclass, the well known single-relaxation-time BGK model [50], is

depleted of this possibility. Hence, the necessity to have, at least, a rough estimate of the stable relationships between all these actors could provide significant savings in the computational time. However, the difficulty of such a study is that the relaxation rates influence the attainable velocity amplitude of the model in a very complex way [37, 40, 52].

In this work we examine the equilibrium parameter range available for binary-liquid free energy model [58]. This multiphase system is described by the Navier-Stokes equation with the advection-diffusion phase propagation equation. The advection-diffusion equation describes the motion of the interface, and it contains the non-linear chemical potential expression through the phase parameter. Phase parameter takes a value of $\pm 1$ in different phases. Based on the phase value, viscosity of simulated liquids can be assigned to different values but density remains uniform across phases, which is one of the limitations of the binary-liquid approach. The interested reader is referred to the comprehensive review for binary-liquid models available by Zheng et al. [68] and recent benchmark simulations [17]. The stability analysis of the whole system is an extremely complicated task because of the non-linearity of the equilibrium functions for the Navier-Stokes, phase field equation and coupling between them. The stability map could drastically improve the robustness of multiphase LBM applications, in particular for microchannel flows where capillary number $Ca$ is typically relatively small and it varies in interval $Ca \approx 0.001 \sim 0.1$. In LBM binary-liquid model,

$$Ca = \frac{U \mu_{liq}}{\gamma}, \tag{1}$$

where $U$ is the reference micro-velocity, $\mu_{liq} = \frac{\rho}{3}\left(\frac{1}{\omega_{liq}} - \frac{1}{2}\right)$ is the kinematic viscosity related to relaxation rate $\omega_{liq} \in ]0, 2[$ of hydrodynamic (Navier-Stokes) LBE scheme, and $\gamma = \sqrt{\frac{8\,k\,A}{9}}$ is the modelled tension coefficient expressed via two positive parameters, $k$ (surface tension parameter) and $A$ (Landau biquadratic free energy model potential parameter). These two parameters also determine the phase propagation equation which is a non-linear advection-diffusion equation where the phase mobility coefficient $\Gamma$ defines diffusion scaling. Therefore, in low capillary number regime, one is interested in keeping the ratio $\frac{\gamma}{\mu_{liq}}$ as large as possible, in order to increase the velocity amplitude and, hence, the computational efficiency of the scheme [38]. This can be achieved either by increasing $\gamma$ or decreasing $\mu_{liq}$, or simultaneously varying the two parameters, but keeping in mind that the stable velocity amplitude decreases with $\mu_{liq}$, in an analytically unknown way, even for single phase BGK NSE simulations. So far, the multiphase stability results are concentrated on numerical observations. In particular, in work [48, 49] it was observed that MRT collision operator may reach larger stability regions for multiphase models. The work by Kendon et al. [35] studied the spinoidal decomposition and examined results withe respect to their dependency on $\gamma$ and $\mu_{liq}$. It was concluded that the best way to obtain larger ratio $\frac{\gamma}{\mu_{liq}}$ relies on the simultaneous decrease $A$

and $k$, thus reducing the surface tension $\gamma$ (see Eq. (1)), but also decreasing $\mu_{liq}$. The liquid viscosity $\mu_{liq}$ should however decrease faster than $\gamma$, the difficulty is in keeping flow stability. At the same time, one should increase the interface mobility diffusion coefficient $\Gamma$ to keep stable interfaces. However, large diffusion coefficients are known to be inaccurate in LBM schemes based on single relaxation time operator and, in binary-liquid models, the increase of the mobility parameter $\Gamma$ leads to the alleviation of the contact line accuracy [48]. This suggests a very complex interplay of all physical and numerical parameters.

In this work, we propose to estimate the available range of parameters that, simultaneously, guarantees stable and sufficiently accurate numerical solutions, based on the stability analysis of the linearized phase propagation equation. This will provide the necessary map in space $\{A, k, \Gamma, U\}$, also depending on the relaxation rates of advection-diffusion LBE scheme involved for phase equation. Aforementioned stability results are obtained through the von Neumann linear analysis. In this approach one substitutes a harmonic function as solution and finds conditions in parameter space where the amplitude is non-growing. Our recent works [23, 29, 37] developed analytically the necessary stability conditions for one-dimensional (D1Q3), two-dimensional (D2Q5,D2Q9) and three-dimensional (D3Q7,D3Q13, D3Q15 and D3Q19) advection-diffusion, isotropic and anisotropic (AADE) models. In parallel, it has been first observed numerically [53, 55] and then rigorously proved [29], that the non-negativity of the equilibrium function is sufficient for stability of the AADE BGK scheme. In the diffusion limit, when velocity vanishes, the non-negativity of the equilibrium function is sufficient for stability of the BGK and TRT AADE schemes for any relaxation rates [29], but also for the anisotropic *linkwise* L-model [24]. Interestingly, this stable TRT/BGK equilibrium parameter map may become destroyed by a blind choice of free MRT relaxation rates, [24]. In the advection limit, the specific combination $\Lambda = \left(\frac{1}{\omega_+} - \frac{1}{2}\right)\left(\frac{1}{\omega_-} - \frac{1}{2}\right) = \frac{1}{4}$ of two relaxation rates (TRT/MRT schemes) may match the optimal stability, where the necessary conditions become sufficient. Beyond this TRT subclass, called "optimal", the stable velocity amplitude depends on the two relaxation rates separately, and the non-negativity conditions are only sufficient when the modeled diffusion coefficient is large enough [37]. The exact dependency of stable velocity with respect to $\{\omega_+, \omega_-\}$ has been only derived for the D1Q3 model, however it also governs the isotropic and link-wise anisotropic multi-dimensional schemes in advection-dominated zone, especially for the minimal models (D2Q5,D3Q7) (see [23, 37]). The non-negativity of the immobile equilibrium weight completes the stability boundary, providing a necessary condition for the minimal and D3Q15 models. Other hydrodynamic velocity sets may shift this diffusion boundary via proper choice of their equilibrium weights. However, their diffusion boundary also narrows towards the non-negativity of the immobile weight increasing the anisotropy of the modeled diffusion tensor, [23, 24].

In this paper we develop the stability analysis of the non-linear phase propagation equation. We restrict ourselves to D1Q3 scheme, keeping in mind that the

necessary stability map of this one-dimensional model should be respected by all others. Moreover, in linear case, the specific multi-dimensional optimal TRT schemes have been able to reach one-dimensional optimal stability. The paper is organized as follows. First, the governing equations and the binary liquid numerical scheme are presented in Section 2. The necessary stability conditions of the D1Q3 BGK phase field scheme are analytically derived in Section 3, based on the linearization of the equilibrium distribution. The results are compared to linear predictions and then confronted to numerical simulations in two limits: pure diffusion and high advection velocities. The advection limit is then re-assessed with the optimal TRT subclass, confirming its ability to retain the optimal stability for non-linear equations. These results are discussed in Section 4. We formulate our findings in a form of simple numerical recipes for the parameters choice in Section 5. They are schematized in Fig. 7. Section 6 concludes the paper. In Appendix A, the linearized, von Neumann stability problem is built for the d1Q3 BGK phase field scheme. Exact von-Neumann solution for its amplification factor is constructed in Appendix B.

## 2. Binary-liquid LBE model

We consider modelling of binary liquid system described by the following system of PDEs [47, 58, 68]:

$$\partial_t \rho + \partial_\alpha \rho u_\alpha = 0 \tag{2}$$

$$\partial_t \rho u_\alpha + \partial_\beta \rho u_\alpha u_\beta = -\partial_\beta P_{\alpha\beta} + \partial_\beta \nu(\partial_\beta \rho u_\alpha + \partial_\alpha \rho u_\beta) \tag{3}$$

$$\partial_t \phi + u_\alpha \partial_\alpha \phi = M \partial^2_{\beta\beta} \mu \tag{4}$$

$$P_{\alpha\beta} = (p_0 - k\phi\partial^2_{\gamma\gamma}\phi - \frac{k}{2}|\partial_\gamma \phi|^2)\delta_{\alpha\beta} + k\partial_\alpha\phi\partial_\beta\phi \tag{5}$$

$$\mu = A(-\phi + \phi^3) - k\partial^2_{\gamma\gamma}\phi \tag{6}$$

$$p_0 = c_s^2 \rho + A(-0.5\phi^2 + 0.75\phi^4), \tag{7}$$

where $P_{\alpha\beta}$ is the momentum flux tensor, $\mu$ is the chemical potential, $M$ is the mobility coefficient (to be defined later through positive parameter $\Gamma$), $k > 0$ is related to the surface tension contribution, and $A > 0$ is the parameter in the Ginzburg-Landau potential. Hereafter, we assume summation for repeating Greek symbols.

These equations describe the binary liquid (multiphase) behaviour with respect to the variable fields: density $\rho$, velocity $\vec{u}$ and indicator function $\phi$. The liquids have uniform density $\rho$, but different kinematic viscosities $\nu_{gas}$ and $\nu_{liq}$, respectively for gas and liquid phases. The relative distribution of two phases is described via the indicator-type continuous function $\phi(\boldsymbol{r}, t) \in [-1, 1]$, with $\phi = 1$ in the liquid phase and $\phi = -1$ in a gas phase. The interface propagation is described by non-linear, advection-diffusion type equation (4), hereafter referred to as the phase field equation. The two-phase state equation extends the ideal gas single-phase relationship $p_0 = c_s^2 \rho$ to account for two-phases co-existence through the biquadratic Ginzburg-Landau potential, Eq. (7).

The binary liquid system is simulated with two sets of distributions via the lattice Boltzmann method. The population set $\{g_i\}$ is responsible for the simulation of the continuity equation (2) and the two-phase Navier-Stokes equations (3). The population set $\{f_i\}$ is responsible for the simulation of the phase-field equation (4). The populations are defined on a regular grid and they are subject to the update rule applied in the predefined directions $\{\boldsymbol{c_i}\}$ using LBE collision operators. The hydrodynamic scheme is coupled with the phase-field scheme via the velocity field (obtained from the the Navier-Stokes solution) and the indicator-function distribution (obtained from the phase-field solution). As simplest example, the single-relaxation-time (BGK) collision operator [50] for both equations reads as :

$$g_i(\boldsymbol{x}+\boldsymbol{c_i},t+1)=g_i^*(\boldsymbol{x},t)\ ,\ g_i^*(\boldsymbol{x},t)=g_i(\boldsymbol{x},t)-\omega_\rho\big(g_i(\boldsymbol{x},t)-g_i^{eq}(\boldsymbol{x},t)\big)\ , \tag{8}$$

$$f_i(\boldsymbol{x}+\boldsymbol{c_i},t+1)=f_i^*(\boldsymbol{x},t)\ ,\ f_i^*(\boldsymbol{x},t)=f_i(\boldsymbol{x},t)-\omega_\phi\big(f_i(\boldsymbol{x},t)-f_i^{eq}(\boldsymbol{x},t)\big)\ , \tag{9}$$

where $f_i^{eq}$ and $g_i^{eq}$ are equilibrium distributions given below by Eq. (12) and Eq. (14), respectively.

The TRT collision operator [21] decomposes the populations and the equilibrium distribution into the symmetric (marked with "+") and antisymmetric (marked with "-") components which are computed once for the pair of opposite directions $(\boldsymbol{i},\bar{\boldsymbol{i}})$:

$$f_i^{\pm}=\frac{f_i\pm f_{\bar{i}}}{2}\ . \tag{10}$$

The symmetric and anti-symmetric equilibrium components $f_i^{eq\pm}$ are prescribed as function of the conserved quantities. The collision is then performed with two independent relaxation rates for symmetric and antisymmetric modes:

$$\begin{aligned}
&f_i^*(\boldsymbol{x},t)=f_i(\boldsymbol{x},t)-\omega_\phi^+(f_i^+-f_i^{eq+})-\omega_\phi^-(f_i^--f_i^{eq-})\ ,\\
&f_{\bar{i}}^*(\boldsymbol{x},t)=f_{\bar{i}}(\boldsymbol{x},t)-\omega_\phi^+(f_i^+-f_i^{eq+})+\omega_\phi^-(f_i^--f_i^{eq-})\ ,\\
&f_i(\boldsymbol{x}+\boldsymbol{c_i},t+1)=f_i^*(\boldsymbol{x},t)\ ,\ \forall\ i\ .
\end{aligned} \tag{11}$$

The BGK operator is the particular subclass of the TRT with $\omega^+_{\{\phi,\rho\}}=\omega^-_{\{\phi,\rho\}}$.

The set of three velocities for the one-dimensional D1Q3 model is represented as $\{c_{ix}\}=\{0,1,-1\}$. The equilibrium function for modelling the Navier-Stokes equation reads as:

$$\begin{aligned}
&g_i^{eq}=3w_i\Big(p_0+\rho u_x c_{ix}+\rho u_x^2\Big)\ \text{for}\ i=1,2\ ,\\
&g_0^{eq}=\rho-\Big(g_1^{eq}+g_2^{eq}\Big)\ ,
\end{aligned} \tag{12}$$

where the macroscopic parameters are calculated as $\rho=\sum_i g_i$, $\rho u_x=\sum_i g_i c_{ix}$, weights $w_i$ take values $\{\frac{1}{6},\frac{1}{6}\}$ for $i=1,2$ and local pressure value $p_0$ is defined by Eq. (7) with $c_s^2\in[0,1]$. The symmetric and anti-symmetric equilibrium components are, respectively,

$$g_1^{eq+}=3w_1\Big(p_0+\rho u_x^2\Big)\ ,\ g_1^{eq-}=\rho u_x\ ,\ g_0^{eq+}=g_0^{eq}=\rho-2g_1^{eq+}\ ,\ g_0^{eq-}=0\ . \tag{13}$$

We note that $g_2^{eq+} = g_1^{eq+}$ and $g_2^{eq-} = -g_1^{eq-}$. Further equilibrium corrections include chemical potential [58].

The equilibrium function for non-linear advection-diffusion scheme reads for the D1Q3 model:

$$\begin{aligned} f_i^{eq} &= w_i\Big(\Gamma\mu + 3\phi u_x c_{ix} + 3\phi u_x^2\Big) \text{ for } i = 1, 2 \ , \\ f_0^{eq} &= \phi - (f_1^{eq} + f_2^{eq}), \end{aligned} \tag{14}$$

where conserved quantity $\phi = \sum_i f_i$, the weights $w_i$ are the same as the hydrodynamic weights: $\{\frac{1}{6}, \frac{1}{6}\}$. Similar as in Eq. (13),

$$f_1^{eq+} = w_1\Big(\Gamma\mu + 3\phi u_x^2\Big) \ , \ f_1^{eq-} = \rho u_x \ , \ f_0^{eq+} = f_0^{eq} = \phi - 2f_1^{eq+} \ , \ f_0^{eq-} = 0 \ . \tag{15}$$

Macroscopic transport parameters are defined with the help of the relaxation rates, as:

$$\begin{aligned} M &= \frac{\Gamma}{3}\Big(\frac{1}{\omega_\phi^-} - \frac{1}{2}\Big) \\ \nu &= \frac{1}{3}\Big(\frac{1}{\omega_\rho^+} - \frac{1}{2}\Big) = \nu_{gas} + \frac{\phi - 1}{2}\big(\nu_{liq} - \nu_{gas}\big), \end{aligned} \tag{16}$$

where $\nu_{liq}$ and $\nu_{gas}$ are prescribed values, rescaling the physical values to lattice units.

The TRT collision operator employs two relaxation parameters for each of two equations. It is convenient to parametrize this additional degree of freedom via the so-called "magic" positive parameter $\Lambda = \Big(\frac{1}{\omega_+} - \frac{1}{2}\Big)\Big(\frac{1}{\omega_-} - \frac{1}{2}\Big)$. This free-tunable parameter controls the effective location of the bounce-back walls [25], second-order accuracy in location of boundary [27] and interfaces [21], spatial accuracy [10, 53], consistency [22] and, to some extent, stability [29, 37, 53]. In particular, $\Lambda = \frac{1}{4}$ achieves the optimal stability for the linear advection-diffusion, isotropic or anisotropic, equation [23, 29]. The optimal stability consists of necessary, advection and diffusion, boundaries, which prove sufficient when $\Lambda = \frac{1}{4}$. Beyond this choice, the necessary conditions may become insufficient, depending on two relaxation rates, and the effective stability boundary becomes rather complex, even for the BGK subclass [37]. On the other side, it has been proved that the non-negativity of the equilibrium values (divided by conserved quantity) is sufficient for the BGK linear advection-diffusion equations, [29]. The non-negativity conditions are much more restrictive than the optimal ones, but they become necessary for the BGK operator when $\omega$ approaches 2 and the diffusion coefficient vanishes (see Appendix B, [37]). In particular, in the next section we will examine if the non-negativity conditions remain sufficient for the linearized phase-propagation equation. We then verify if the optimal TRT subclass $\Lambda = \frac{1}{4}$ keeps its distinguished stability property.

## 3. Stability analysis of the phase field BGK scheme

We analyze the stability of the BGK scheme assuming $\omega = \omega_\phi^+ = \omega_\phi^-$ in Eq. (11), along with the equilibrium function (14). This scheme solves for the one-dimensional non-linear binary-liquid phase equation:

$$\partial_t \phi + u_x \partial_x \phi = M \partial_{xx}^2 \mu. \tag{17}$$

### 3.1. *Linearization*

To perform von Neumann stability analysis of the scheme, the equilibrium function (14) has to be linearized with respect to the non-linear dependency $\mu(\phi)$. This can be obtained by imposing a small perturbation, assuming steady-state conditions [40] around $\phi_0 = \pm 1$: $\phi = \phi_0 + \delta\phi$. Von Neumann analysis implies the substitution of the Fourier functions as solutions for unknown functions. Thus, the phase variation in space can be expressed as:

$$\delta\phi_{\pm m} = \delta\phi e^{\pm \boldsymbol{i} m k_x c_{ix}}, \tag{18}$$

where $\phi_{\pm m}$ is the phase function value at the node located at the distance $\pm m$ grid spacings from the specific node and $k_x$ is wave number. The laplacian of the phase parameter in Eq. (14) can be transformed via the central-difference scheme:

$$\Delta\delta\phi = \delta\phi_1 - 2\delta\phi + \delta\phi_{-1} = \delta\phi(e^{k_x} + e^{-k_x} - 2) = 2\delta\phi(\cos(k_x) - 1) \tag{19}$$

After linearization and substitution of the Fourier mode into Eq. (14), the linearized equilibrium function takes the form:

$$\begin{aligned} &\delta f_i^{eq} = 3 w_i \delta\phi \Big( \Gamma\big(A(3\phi_0^2 - 1) - 2k(\cos(k_x) - 1)\big) + c_{ix} u_x + u_x^2 \Big) \ , \ i = 1, 2 \ , \\ &\delta f_0^{eq} = \delta\phi - (\delta f_1^{eq} + \delta f_2^{eq}). \end{aligned} \tag{20}$$

By prescribing the Fourier modes: $f_i(\boldsymbol{r} + \boldsymbol{c_i}, t+1) = \Omega f_i(\boldsymbol{r}, t) e^{\boldsymbol{i} k_x \cdot c_{ix}}$ with the amplification factor $\Omega$, one obtains the following von Neumann linear problem

$$\Omega \mathcal{F} \delta F = \mathcal{L} \delta F, \tag{21}$$

where $\delta F$ is the eigenvector, $\mathcal{F}$ is the frequency matrix specified by Eq. (A.1) and $\mathcal{L}$ is the collision matrix for linearized equilibrium, specified by Eqs. (A.2)-(A.3) for the linearized BGK operator with Eq. (14).

The linear numerical scheme is stable in von Neumann sense when the amplitudes of all the roots $\Omega$ are found inside the unit circle. In particular, the D1Q3 model has three roots $\Omega$ in Eq. (21) and analysis of their amplitudes is complicated. However, it is possible with the help of the Miller's theorem [44] to sequently reduce the $n-$order polynomial equation to the linear equation that has the same stability properties as the initial equation. Proceeding this way, the analytical parameter map where $|\Omega(c_e, u_x, \omega_+, \omega_-, k_x)| = 1$ is constructed in work [37] for the D1Q3 TRT/BGK ADE linear schemes, using the following equilibrium function:

$$f_i^{eq} = 3 w_i \phi \Big( c_e + u_x c_{ix} + u_x^2 \Big) \ , \ i = 1, 2 \text{ and } f_0^{eq} = \phi(1 - c_e - u_x^2). \tag{22}$$

This equilibrium is suitable for modeling of one-dimensional linear advection-diffusion equation

$$\partial_t \phi + u_\alpha \partial_\alpha \phi = D \partial^2_{\beta\beta} \phi. \tag{23}$$

The modeled diffusion coefficient $D$ is equal to $c_e\left(\frac{1}{\omega_-} - \frac{1}{2}\right)$ where equilibrium parameter $c_e$ is free but restricted to interval $[0, 1]$. The velocity boundary $|u_x(c_e, \omega_+, \omega_-)|$ was established such that this is the minimal velocity value over all $k_x$ where $|\Omega(c_e, u_x^2, \omega_+, \omega_-, k_x)| = 1$.

The BGK collision operator with the relaxation rate $\omega$ is addressed in the rest of this section. The equilibrium function (20) of the linearized phase equation fits the equilibrium (22) for the linear advection-diffusion equation if we set $c_e$ equal to $c_e^{nonlin}$:

$$c_e \to c_e^{nonlin} = \Gamma(A(3\phi_0^2 - 1) - 2k(\cos(k_x) - 1)) \, . \tag{24}$$

The principal difference with the linear case is that $c_e^{nonlin}$ depends on $k_x$, because of the non-linearity of the original phase equation, and then the previous results do not formally apply. As in the linear case, we divide the analysis into pure diffusion and advection limits, then combine both conditions and compare them, first, with linear stability results and, second, direct numerical computations.

### 3.2. *Pure diffusion equation of phase field*

#### 3.2.1. *Von Neumann stability analysis*

When velocity is set equal to zero, pure diffusion equation of phase field reads

$$\partial_t \phi = M \partial^2_{\beta\beta} \mu. \tag{25}$$

It has been proved [29] that the positivity of all equilibrium distribution $f_i^{eq}/\phi$ guarantees stability of pure-diffusion linear TRT schemes. Assuming $c_e > 0$, this condition is satisfied by the D1Q3 model when immobile weight is non-negative, i.e. when $c_e$ belongs to interval $[0, 1]$:

$$0 \le c_e \le 1. \tag{26}$$

Formally, von Neumann stability analysis sets this condition when $k_x = \pi$ (see Eq.(61) in [29]). In turn, $k_x = \pi$ yields the maximal value for $c_e^{nonlin}$:

$$\max c_e^{nonlin} = 2\Gamma(A + 2k) \, . \tag{27}$$

Non-negativity condition (26) is then satisfied for $c_e^{nonlin}(k_x = \pi)$ providing that

$$0 \le A + 2k \le \frac{1}{2\Gamma} \, , \; A > 0 \, , \; k > 0 \, , \; \Gamma > 0 \, . \tag{28}$$

Both the necessity and sufficiency of condition (28), with respect to the stability of the BGK scheme featuring the linearized equilibrium (20), can be proved rigorously as presented below.

The characteristic equation for the linearized problem, Eq. (21), is discussed in Appendix A. Appendix B applies the Miller's Theorem 6.1 [44] to estimate its von Neumann stability bounds, reducing the third-order characteristic equation to a linear one. The amplitude of the root of this linear equation is given by Eq. (B.1). Applying this result, the linearized diffusion scheme with $\phi_0 = \pm 1$ and $u_x = 0$ is stable provided that $|\Omega| \in [0,1]$ , $\forall k_x$, $|\Omega|$ is given by the following relation:

$$\begin{aligned} |\Omega| &= \frac{a}{b} \ , \\ a &= m^4\left(-4a\Gamma((\omega-1)\Omega+1) - 8\Gamma k((\omega-1)\omega+1) + \omega^2\right) + \\ &\quad 2m^2(-2a\Gamma((\Omega-1)\omega+1) + (\omega-2)\omega+2) + (\omega-2)^2 \ , \\ b &= m^4\left(-4\gamma\omega(a+2k) + 4\Gamma(a+2k) + \omega^2\right) + \\ &\quad 2m^2(-2a\Gamma(\omega-1) + (\omega-2)\omega+2) + (\omega-2)^2 \ , \ m = \tan\Big(\frac{k_x}{2}\Big) \ . \end{aligned} \tag{29}$$

We confirm with the help of optimization routines [65] that condition $\Omega^2 \leq 1 \ \forall m$ is guaranteed with condition (28). Note that this condition becomes then necessary and sufficient, and it is independent of the relaxation rate.

### 3.2.2. *Numerical simulations*

Numerical simulations were performed for the pure diffusion non-linear phase equation (25). The phase field was initialized as:

$$\phi(x,0) = \begin{cases} 1, & \text{for } j \in ((N_x-1)/2 - W/2, (N_x-1)/2 + W/2) \\ -1, & \text{otherwise,} \end{cases} \tag{30}$$

where $W = 20$ is the width of the droplet, $j$ is the grid node number, $j = 1, \ldots, N_x = 129$. The simulations were run for $10^3$ iterations. They were considered as unstable if NaN values were detected for $\phi$. Examples of the phase field profiles for the pure diffusion and advection cases are plotted in Fig. 1, with $\phi = 1$ for "liquid" and $\phi = -1$ for "gas". This figure illustrates that the binary-liquid model is a diffusive interface model, where the interface is a smooth transition between two phases.

Figure 2 compares then numerical and theoretical stability map in parameter space $A(k, \omega)$. We observe, in agreement with the predictions above, that the numerical and theoretical area given by Eq. (28) practically coincide for different relaxation rates, except for $\omega = 1.99$ where the stable area slightly reduces. In fact, $\omega = 1.99$ approaches the linear stability limit $\omega = 2$. It has been already detected for highly non-linear transport equation in variably saturated soil [31] that the linearized analysis may become deficient in this eigenvalue limit. The two diagrams in Fig. 2 also confirm that the stable area linearly scales with $\Gamma^{-1}$, exactly as predicted by the non-negativity condition (28). One can then suggest that this property remains also valid in the presence of advection, because of equivalent condition (24), at least so far as the stable parameter area scales with $c_e$.

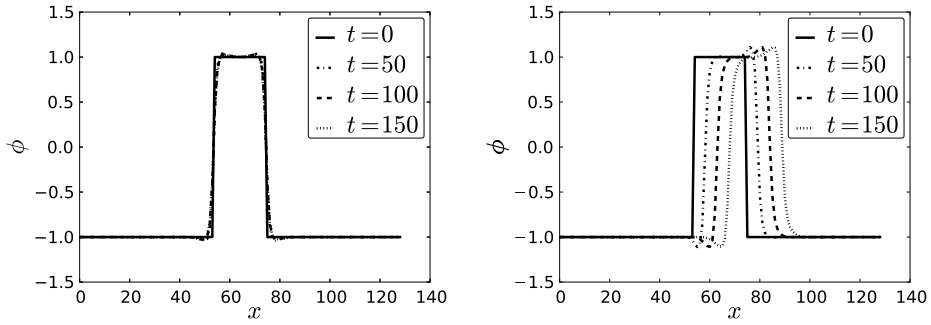


Fig. 1. The phase profile and its evolution is shown after $0, 50, 100, 150$ iterations. $\phi = 1$ is corresponding to "liquid", $\phi = -1$ is corresponding to "gas". Left figure is pure diffusion case, $u_x = 0$, right picture is for $u_x = 0.1$. Other parameters were taken as $\Gamma = 1$, $\omega = 1$, $A = 0.04$, $k = 0.04$.

In resume, the exact analysis of the linearized pure diffusion problem produces the same, necessary and sufficient, stable parameter range as the non-negativity condition applied for diffusion equilibrium parameter $c_e^{nonlin}$ when $k_x = \pi$. This result is confirmed by numerical simulations of the underlying non-linear problem, except very close to stability limit of the relaxation rate where the stable area narrows.

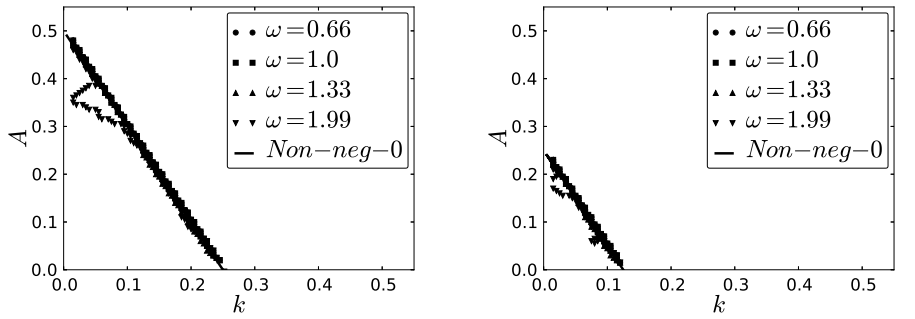


Fig. 2. Left ($\Gamma = 1$) and right ($\Gamma = 2$) diagrams compare stability area obtained numerically for the pure diffusion equation with the theoretical prediction given by Eq. (28), in wide range of relaxation parameter $w$. The stable region $A(k)$ is below the points.

### 3.3. *The advection-diffusion equation*

This section develops analysis of the phase propagation equation in the presence of the advection. The objective is to establish the stable parameter range for $|u_x|$ versus other equilibrium parameters, as $A$, $k$ and $\Gamma$, and relaxation rate $w$. The works [29,

37, 53, 55] perform exact and numerical von Neumann stability analysis for the linear advection-diffusion TRT/BGK schemes. In particular, it has been proved [29] that the non-negativity of the whole set of equilibrium functions, $\{\frac{f_i^{eq}}{\phi}\}$, is sufficient for the stability of the BGK linear mass-conserving scheme for all velocity sets usually used. This result is valid for any $\omega$ and it becomes necessary in the limit $\omega \to 2$ (see Appendix B [37]). Thus, if the equilibrium populations divided by conserving quantity are all non-negative, it is guaranteed that the BGK linear ADE scheme is stable, in the periodic domain without boundaries and sources, at least. Therefore, the limit $\omega \to 2$ is expected to be most unstable for the BGK model.

The exact stability curves $|u_x(c_e, \omega)|$ have been established in work [37] for D1Q3 model. They present much less strong constraints than those given by the non-negativity conditions when $\omega$ is far enough from stability limit $\omega = 2$, but they are more complicated to use. The (limited range) approximation of the exact curves is proposed in work [31]. In practice, exact stability curves approach very closely the non-negativity condition for mobile populations when $w \geq\approx 1.99$ (see Fig. 4 in work [37]). In current work, we first examine if the simple non-negativity conditions still provide realistic stability range for the non-linear problem. For this purpose, we re-interpret them for the linearized equilibrium and then compare obtained predictions to numerical simulations. In parallel, we develop semi-analytical analysis of the characteristic equation given in Appendix A to verify sufficiency of non-negativity conditions for a wide range of relaxation rate and their necessity in the limit $\omega_\phi \to 2$.

### 3.4. *Non-negativity conditions*

The non-negativity equilibrium conditions for the D1Q3 linear advection-diffusion scheme, Eq. (22), are provided by two constraints [29, 37, 55]:

$$\begin{cases} u_x^2 \leq 1 - c_e \ , \ c_e \in [0,1] \ , \\ u_x^2 - |u_x| + c_e \geq 0 \ . \end{cases} \tag{31}$$

Again, first condition guarantees the non-negativity of $f_0^{eq}/\phi$ for immobile population. It reduces to pure diffusion constraint $c_e \in [0,1]$ for zero velocity. The second condition guarantees the non-negativity, as $(f_i^{eq}/\phi) > 0$, for two moving populations. The stable map $u_x(c_e)$ predicted by these conditions is illustrated in Fig. 3, following work [29].

Let us first formally replace $c_e$ with $c_e^{nonlin}$ for linearized phase equation (24), then:

$$|u_x|(1 - |u_x|) \leq c_e^{nonlin} \leq 1 - u_x^2 \ , \ c_e^{nonlin} \in [0,1] \ . \tag{32}$$

We keep in mind that the conditions derived for $k_x = \pi$ in pure diffusion case were sufficient. The maximal value of $c_e^{nonlin}$ over $k_x$ corresponds to $k_x = \pi$ and it is set by Eq. (27). Therefore, one can conclude that non-negativity conditions necessarily

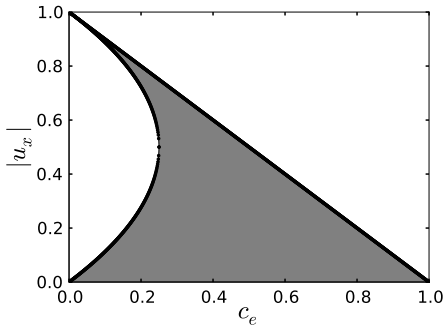


Fig. 3. The non-negativity area $\frac{f_i^{eq}}{\phi} > 0$ for linear equilibrium distribution (22) of the D1Q3 model is shaded. It presents sufficient condition valid for $\forall\omega$ in case of the BGK scheme. This parameter map is necessary to respect when $\omega \to 2$.

yield:

$$\frac{|u_x|(1-|u_x|)}{2\Gamma} - 2k \leq A \leq \frac{1-u_x^2}{2\Gamma} - 2k \ , \ k_x = \pi \ . \tag{33}$$

Note that the upper boundary then guarantees the non-negativity of the immobile weight for any $k_x$. However, the lower boundary may narrow, in principle. The difficulty is that the limiting stability value $k_x$ may become $c_e-$dependent. So far, non-negativity condition $|u_x|(1-|u_x|) \leq c_e$ is asymptotically reached when $\omega \to 2$ and $\cos(k_x) = c_e - 1$ (Eq.(B.3) in work [37]). If we assume that the same situation takes place for the linearized equilibrium, we obtain, plugging $\cos(k_x) = c_e^{nonlin} - 1$ into Eq. (24) and then equating obtained expression to $c_e^{nonlin}$:

$$\begin{aligned} c_e^{nonlin} &= \Gamma(2A - 2k(\cos(k_x) - 1))|_{\cos(k_x)=c_e^{nonlin}-1} \ , \ \text{ then} \\ c_e^{nonlin} &= \frac{2\Gamma(A+2k)}{1+2\Gamma k} \ . \end{aligned} \tag{34}$$

Substitution of this expression into non-negativity condition $|u_x|(1-|u_x|) \leq c_e^{nonlin}$ yields (keeping diffusion upper boundary):

$$\frac{|u_x|(1-|u_x|)}{2\Gamma} - 2k + k|u_x|(1-|u_x|) \leq A \leq \frac{1-u_x^2}{2\Gamma} - 2k \ , \tag{35}$$

In fact, this condition increases the lower boundary by positive quantity $k|u_x|(1-|u_x|)$ and thus narrows the stable area $A(k)$. It can also slightly modify the scaling of the stable domain with $\Gamma$. Below we will examine the validity of conditions (33) and (35) via semi-analytical analysis of the characteristic equation.

### 3.5. *Semianalytical approach*

The necessary and sufficient stability conditions are set when the amplitude of $\Omega$ given by Eq. (B.1) is restricted to interval $[0, 1]$ for all values of wavenumber

$k_x \in [-\infty, \infty]$. In the presence of all parameters, this problem becomes quite complicated to find an exact solution. We then construct the stable parameter space semi-analytically. Namely, we discretize parameter space $(A_i, k_j) \in [0, 0.5] \times [0, 0.5]$ and look for such pairs $(A_i, k_j)$ where $\max_{m\in\Re} |\Omega(m, u_x, \omega, \Gamma = 1, A_i, k_j)|^2 \leq 1$, $\forall\ m = \tan\left(\frac{k_x}{2}\right)$, for fixed values of the relaxation parameters $\omega$ and velocity $u_x$. The solution is constructed with the help of software tool [65].

We note that the linear equilibrium (20) and the hydrodynamic equilibrium (12) for one-phase Navier-Stokes equation, with $p_0 = c_s^2\rho$, have the same form. It follows that conditions (31) also provide its non-negativity conditions replacing $c_s^2$ by $c_e$. In particular, for typical value of sound velocity $c_s = \frac{1}{\sqrt{3}} \approx 0.57735$ they restrict velocity $u_x$ to interval $[0, 1 - c_e \approx 0.650115]$. This value is larger than the incompressible limit $u < c_s$. We prescribe velocity $u_x \in [0, 0.5]$. In linear case, the interval $c_e \in [0, |u_x|(1 - |u_x|)]$ becomes unstable when $\omega \to 2$, namely, $c_e \in [0, 3/16]$ and $c_e \in [0, 0.25]$, respectively, when $|u_x| = 0.25$ and $|u_x| = 0.5$.

The obtained stable domains are plotted in Fig. 4, in the same parameter range for $\omega$ as in numerical simulations below. As expected, the upper boundary approaches the non-negativity condition of the immobile population $f_0^{eq}/\phi$ (see Eq. (33)). Note, however, that we observe a slightly larger area, e.g., for $\omega = 1$ when $u_x = 0.25$ (left upper diagram). This indicates that in the presence of velocity, the linearized problem does not have identical behaviour with the linear one by simply replacing $c_e$ with $c_e^{nonlin}$, because of the angular dependency in $c_e^{nonlin}$. However, similar to linear stability analysis, the diffusion non-negativity boundary remains sufficient. In linear case, we expect that the advection (lower) boundary appears when $\omega > 2(3 - \sqrt{6}) \approx 1.10102$. This value corresponds to boundary $(\frac{1}{\omega} - \frac{1}{2})^2 = \frac{1}{6}$ where the BGK model losses the *extended* optimal stability which is controlled by diffusion line (see [37]). The largest unstable interval in the limit $\omega \to 2$ have been indicated above: $c_e \in [0, 3/16]$ when $u_x = 0.25$ and $c_e \in [0, 0.25]$ when $u_x = 0.5$. Figure 4 shows that lower advection boundary appears for $\omega = 1.7$ when $u_x = 0.25$ and $\omega = 1.33$ when $u_x = 0.5$. This boundary approaches the predicted non-negativity limit given by Eqs. (33), and then, when $\omega \to 2$, slightly narrows this stable interval $c_e^{nonlin}$ towards one predicted by Eqs. (35). In fact, the two conditions (33) and (35) are very close for these two velocity values. On the whole, the semianalytical analysis of the linearized problem confirms the predictions obtained by direct applications of the linear analysis results to $u_x(c_e^{nonlin})$. Moreover, the non-negativity lines predicted for $k_x = \pi$ and $k_x = c_e - 1$ remain (almost) sufficient for the considered velocity values in the whole range of relaxation rates.

In next section, we confront these results to direct numerical simulations.

#### 3.5.1. *Numerical approach*

In this section we examine stable parameter range established by numerical simulations of the advection-diffusion phase propagation equation. We compare these numerical results with conditions (33) based on the non-negativity conditions for

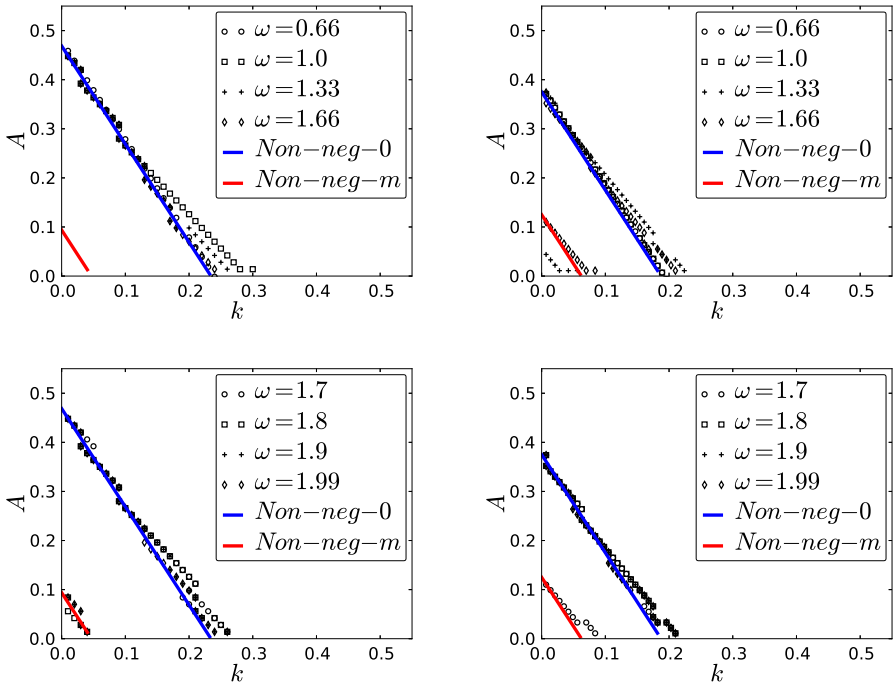


Fig. 4. The semianalytical results for the phase field equation are build with $\Gamma = 1$, when $(A, k) \in [0, 0.5] \times [0, 0.5]$ and $u_x = \{0.25, 0.5\}$ (from left to right), in the range of relatively small values $\omega \in [0.33, 1.66]$ and their large values $\omega \in [1.7, 1.99]$ (from top to bottom). The stable area for each $w$ is below the upper (diffusion) line and above the lower (advection) line when the latter is present. Non-negativity limits are plotted for Eq. (33). Color online.

$\max c_e^{nonlin}$. The simulation domain, parameter range and numerical stability criteria are the same as for the pure-diffusion equation above. We perform a series of simulations for $\Gamma = 1$ and $u_x = \{0.25, 0.5\}$ assuming that stable domain $A(k)$ varies linearly with $1/\Gamma$ (see Eq. (28)). This assumption was confirmed numerically. The obtained stable areas in parameter space $(A, k)$ are shown in Fig. 5 in two intervals of relaxations parameter: $\omega \in [0.33, 1.66]$ in the top row, and $\omega \in [1.7, 1.99]$ in the bottom row. The numerical bounds are plotted together with the non-negativity conditions (33). The two diagrams in the top row, for $u_x = 0.25$ and $u_x = 0.5$, show that the stable numerical boundary slightly narrows the necessary stability condition: $u_x^2 = 1 - c_e^{nonlin}$ dictated by the non-negativity of the immobile weight. In turn, as could be expected from the linear stability results [37], the non-negativity condition for moving populations is unnecessary restrictive in this range of the relaxation rates (see Fig. 5) and the advection boundary only appears for larger $\omega$ values (see two bottom diagrams). Moreover, the stable numerical area then reduces inside the non-negativity interval (33) such that the sub-domain high $A$ - low $k$ be-

comes unstable. The stable domain further reduces increasing velocity. Note that the semi-analytical analysis of the linearized equation only detected a weak worsening described by Eq. (35). We should then attribute the numerical deterioration of stability for large values $\omega$ to non-linear effects, and in particular, to interface stability as depicted in Fig. 7.

In resume, the numerical simulations therefore suggest that the non-negativity conditions established for $\max c_e^{nonlin}$ provide reasonable parameter space for the non-linear advection-diffusion equation with large advection velocities only when the relaxation parameters are sufficiently small, $\omega \leq\approx 1.6$. In this range, the diffusion boundary is almost sufficient. Otherwise, when $\omega$ increases to 2, one first should respect the lower non-negativity boundary in Eq. (33) or Eq. (35) selecting $A$, $k$, $\gamma$ and velocity scale. These conditions may however become insufficient in the non-linear case when $\omega$ is large and the stable domain may then further narrow with the velocity amplitude.

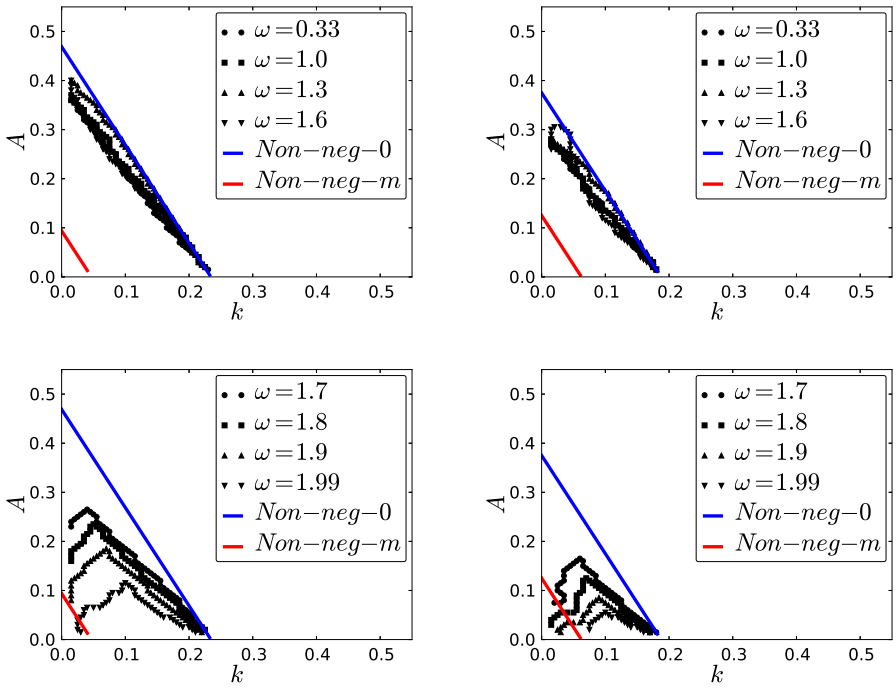


Fig. 5. The stable domain (inside the lines) is obtained by numerical simulations for $\Gamma = 1$ when $u_x = 0.25$ (left diagrams) and $u_x = 0.5$(right diagrams). Top row addresses the relatively small values of relaxation parameter, $\omega \in [0.33, 1.66]$ . Bottom row: $\omega \in [1.7, 1.99]$. Non-negativity limits are plotted for Eq. (33). Color online.

## 4. The optimal TRT parameter

So far the results allow to explain the numerical observations by Kendon et al. [35]. Namely, it is indicated that the decrease in kinematic viscosity implies the decrease of parameters $k$ and $A$, with a simultaneous increase of $\Gamma$. In fact, the increase of $\Gamma$ is dictated by the phase propagation equation which needs to keep the interface adjusted due to less viscous liquid. The analysis above shows that increase in $\Gamma$ inevitably implies the decrease of the surface tension via parameters $k$ and $A$, thus limiting the available range of stable parameters.

We note that the same goal can be reached by increasing the whole mobility parameter $M = \frac{\Gamma}{3}\left(\frac{1}{\omega_\phi} - \frac{1}{2}\right)$ by decreasing $\omega_\phi$ for same $\Gamma$. Let us drop index $\phi$ as only phase propagation equation is studied, i.e., $\omega_+ = \omega_\phi^+$ and $\omega_- = \omega_\phi^-$ in what follows. As it was indicated (see [23, 28, 31]), the accuracy of the lattice Boltzmann method depends on the quantity $\left(\frac{1}{\omega} - \frac{1}{2}\right)^2$. Thus, the strong decrease of $\omega$ is undesirable for accuracy. This accuracy issue is also indicated in a work by Pooley et al. [47] where the simulation contact angle show larger deviations with the increase of the mobility parameter $M$. Thus, using the BGK collision operator, one should either compromise the stable parameter range $A(k)$, or the accuracy, decreasing $\omega$.

The TRT collision operator has an additional degree of freedom, i.e. $\omega_+$. With its help, the TRT may increase $\omega_-$ keeping the spatial accuracy for fixed specific combination $\Lambda$ of two rates. Also, as demonstrated in works [29, 37], the advection boundary can be avoided by the TRT collision when $\Lambda = \frac{1}{4}$ or using extended dependency $\Lambda(\omega_-)$ (see details in works [23, 29, 37]). In general, the optimal stability is kept for $\Lambda = \frac{1}{4}$, where:

$$\begin{aligned} &\Lambda = \Big(\frac{1}{\omega_+} - \frac{1}{2}\Big)\Big(\frac{1}{\omega_-} - \frac{1}{2}\Big) = \frac{1}{4}\ , \text{ then} \\ &\omega_+ + \omega_- = 2. \end{aligned} \tag{36}$$

The BGK collision operator enters the optimal subclass with $\omega_\pm = \omega = 1$. In case of D1Q3 model, the optimal stability means that the stable area is only bounded by the diffusion boundary, then Eq. (31) reduces to one condition:

$$u_x^2 \le 1 - c_e\ ,\ c_e \in [0,1]\ ,\ \forall\ \omega_\pm\ \text{ if } \Lambda = \frac{1}{4}\ . \tag{37}$$

It follows that the optimal TRT subclass allows to use very small values $c_e$ for any relaxation diffusion value $\omega_-$. The non-linear advection-diffusion equation transforms this condition to upper (pure diffusion) boundary (33), or $c_e^{nonlin} \le 1 - u_x^2$, then:

$$0 \le A \le \frac{1 - u_x^2}{2\Gamma} - 2k\ . \tag{38}$$

Figure 6 shows the stability maps for TRT numerical simulations when $\Lambda = \frac{1}{4}$. The numerical simulations were performed on the same grid and with the same stability criteria as above with the BGK model. To match the BGK parameters, we apply

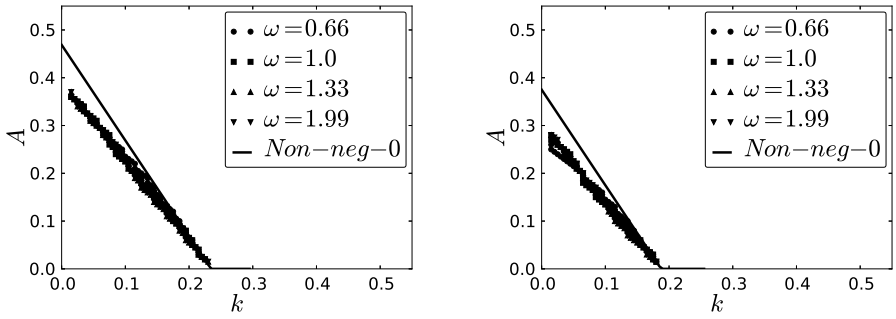


Fig. 6. The numerical simulations with the TRT scheme using optimal stability parameter $\Lambda = \frac{1}{4}$ or $\omega_+ + \omega_- = 2$. The left diagram is for $u_x = 0.25$, the right diagram is for $u_x = 0.5$. One can see that the stability is very similar for all $\omega_- = \omega$. The upper line yields the positivity of the immobile equilibrium population, as prescribed by Eq. (38).

$\omega_- = \{0.33, 0.66, 1.33, 1.66, 1.99\}$. The free relaxation parameter is $\omega_+ = 2-\omega_-$. We observe that the diffusion line slightly narrows condition (38). This is similar to BGK simulations in Fig. 5 for relatively small $\omega$. The distinguished point that this stability diagram is destroyed for BGK model increasing $\omega$ towards 2, while it is kept for all $\omega_-$ using the TRT model with $\Lambda = \frac{1}{4}$. Moreover, in agreement with the predictions of linear stability analysis, the advection line does not appear and the stable domain remains large. Remarkably, this, almost optimal, stable domain is independent of the relaxation rates, in agreement with theoretical predictions for diffusion-dominated boundary, and it scales with $\Gamma$. In case of small diffusion values $\omega_- << 1$, accuracy of truncation corrections and, especially, boundary conditions [31], is maintained when $\Lambda$ remains, roughly, in interval $\approx ]0, 1]$.

## 5. Recommendations

### 5.1. *BGK collision operator*

From the analytical and semianalytical derivations one can see that the non-negativity conditions for all equilibrium values have to be respected when $\omega \to 2$. In the practical multiphase simulations, the parameters $k$ and $A$ are connected through the interface width as $l \approx 5\sqrt{\frac{k}{A}}$. The usual interface width for multiphase simulations is around $3-5$ cell spacings. The larger widths of the interface do not provide enough accuracy for droplet-wall, droplet-droplet interaction [38, 39]. The smaller width of the interface are unstable. Therefore, the two conditions $l = 3$ and $l = 5$ provide two additional lines: $A \approx 2.8k$ and $A = k$. Figure 7 plots recommended

stability region:

$$\begin{aligned} A + 2k &\leq \frac{1 - u_x^2}{2\Gamma} \\ A + 2k &\geq \frac{u_x(1 - u_x)}{2\Gamma} \\ A &\leq 2.8k \\ A &\geq k \, . \end{aligned} \tag{39}$$

A comparison of simulations in Figs. 5 and 7 suggests that it is undesirable to have $\omega \geq\approx 1.6$ for velocities of $u_x \geq 0.25$ as it results in stable domains lying below line $A = k$, where interface width becomes too large. This further constraints the parameter space since one needs to increase the mobility parameter $M = \frac{\Gamma}{3}\left(\frac{1}{\omega} - \frac{1}{2}\right)$ for low viscosities. This can be done only by increasing $\Gamma$, as one cannot decrease $\omega$ towards 0 because of accuracy in the frame of the BGK operator. We recall that the increase of $\Gamma$ reduces the region for parameters $A$ and $k$. As the guideline, one needs to use $\omega \leq\approx 1.6$, and for given $\Gamma$, select parameters $A$ and $k$ in their region presented in Fig. 7.

### 5.2. *TRT collision operator*

For the non-linear phase propagation tests considered herein, the optimal TRT collision operator $\Lambda = \frac{1}{4}$ keeps its optimal linear stability in advection zone (see Fig. 6). That means that the advection (lower) boundary vanishes and the stable domain is almost guaranteed by the non-negativity of the linearized immobile weight, equally for all diffusion relaxation rates $\omega_-$. The TRT operator then allows for much larger stable parameter range $A(k)$ using large values $\omega_-$, also offering the possibility to decrease $\omega_-$ without any drastic sacrifice in accuracy. Therefore, using the optimal TRT subclass, one can find a compromise whether increasing mobility with the help of $\Gamma$ or by reducing $\omega_-$. Future work needs to verify if the *extended optimal subclass* [23, 37] keeps its properties for non-linear problems. This would allow to reduce $\Lambda$ from $\frac{1}{4}$ to $[\frac{1}{8}, \frac{1}{4}]$ when the diffusion coefficient increases. We recall that two particular values, $\Lambda = \frac{1}{12}$ and $\Lambda = \frac{1}{6}$ annihilate the truncation corrections in space, for the third (advection) and fourth (diffusion) order, respectively [23]. Since the modeling of the binary system may require to increase the mobile diffusion coefficients with $\omega_\phi^-$, the use of $\Lambda < \frac{1}{4}$ could further improve for accuracy while retaining optimal stability.

## 6. Conclusion

This work was intended to better understand the stability mechanism behind non-linear problems. Our start point was the highly nonlinear one-dimensional phase-propagation equation of the binary-liquid multiphase LBE model. Its one-dimensional stability bounds established in equilibrium parameter space are necessary to respect in multi-dimensions. Especially, this stable parameter range is

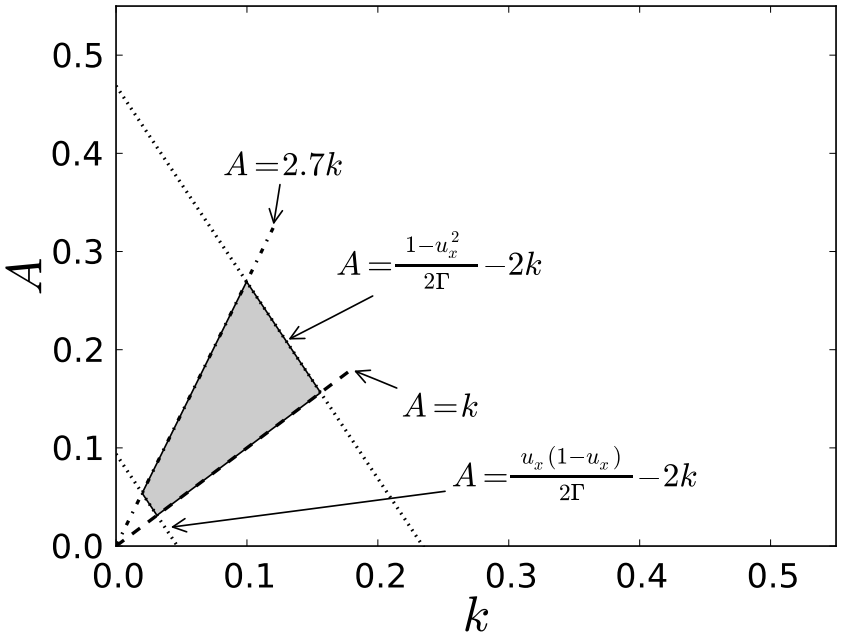


Fig. 7. Sketch of recommended stability area as bounded by four curves, Eq. (39). The lower left and upper boundaries are predicted by the non-negativity conditions Eq. (39) for linearized equilibrium, the curves coming through zero maintain reasonable interface thickness. Expected, that the BGK operator matches this diagram when $\omega <\approx 1.6$, and the optimal TRT subclass keep it for all $\omega_-$, dropping the lower non-negativity boundary.

important for simulations in a low capillary number region. The main outcome of this work is that one can reasonably adapt the principal results of linear stability analysis [29] of the BGK and TRT operators to non-linear problems, and to explain numerical observations. The following summarizes the main findings of this work:

First, the linearized BGK collision operator for phase field equation is analyzed through the linear stability von Neumann analysis and numerical simulations. This shows that the positivity of the immobile equilibrium weight, namely $f_0^{eq}/\phi$, dictates the attainable parameter range for $A$, $k$ and $\Gamma$ via their specific combination obtained from the linearization of the equilibrium. This suggests that the area $(A, k)$ mainly scales as $\Gamma^{-1}$ and explains the numerical observations by Kendon et al. [35]. At the same time, the positivity of the moving equilibrium values, $f_i^{eq}/\phi$, is only required when the relaxation parameter $\omega$ increases and velocity amplitude is relatively large. These two results exactly follow the conclusions for linear equations. However, when $\omega \to 2$, i.e., the relaxation rate approaches

its physical stability limit where the mobility coefficient vanishes, the non-negativity conditions become insufficient, most likely because of complex angular dependency of non-linear effects and the interface growth. On the whole, combining stability and accuracy restrictions for interface width, the stable domain $A(k)$ is very restrictive increasing $\Gamma$ for the BGK operator. This increase is required to keep interface for small kinematic viscosities. At the same time, the optimal TRT collision operator keeps its stable areas independent of the diffusion relaxation rates. They are almost guaranteed by the non-negativity condition for immobile weight alone. Therefore, on the one side, the TRT offers larger stable areas $A(k)$ for all diffusion rates. On the other, it allows to decrease the diffusion rate $\omega_-$ with no impact on the spatial accuracy, and then to increase mobility by keeping the map $(A, k, \Gamma)$.

This work only makes the first step providing necessary relationships in space $\{A, k, \Gamma, U, \omega\}$. The next step will consist in a search of the relaxation rates for the involved LBE hydrodynamic scheme, to achieve the desired velocity amplitude. This could extend and combine the NSE MRT stability analysis [40, 52], the recent ADE TRT/BGK analysis [37] and the linearized chemical potential equilibrium developed in this work. Further work also needs to extend linear multi-dimensional stability analysis [23, 29] to non-linear problems. In particular, we hope that the multi-dimensional non-linear extended optimal TRT ADE schemes will also retain their stability. In such a case, the results derived in this work for one-dimensional model will describe their stable parameter range, as well.

## Appendix A.

The matrices for the linear analysis of D1Q3 linearized scheme are specified as:

$$F = \begin{pmatrix} 1 & 0 & 0 \\ 0 & e^{ik_x} & 0 \\ 0 & 0 & e^{-ik_x} \end{pmatrix} \tag{A.1}$$

and

$$A = \begin{pmatrix} A_1 & A_2 & A_3 \end{pmatrix}, \tag{A.2}$$

where

$$A_1 = \begin{pmatrix} -\omega\left(A\Gamma\left(3\phi_0^2-1\right)+\Gamma k+u_x^2+\Gamma k\omega\cos(k_x)\right)+1 \\ \frac{1}{2}\omega\left(A\Gamma\left(3\phi_0^2-1\right)-\Gamma k\cos(k_x)+\Gamma k+u_x^2+u_x\right) \\ \frac{1}{2}\omega\left(A\Gamma\left(3\phi_0^2-1\right)-\Gamma k\cos(k_x)+\Gamma k+(u_x-1)u_x\right) \end{pmatrix}$$
$$A_2 = \begin{pmatrix} \omega\left(\Gamma\left(-3A\phi_0^2+A-k\right)+\Gamma k\cos(k_x)-u_x^2+1\right) \\ \frac{1}{2}\left(\omega\left(\Gamma\left(3A\phi_0^2-A+k\right)+u_x^2+u_x-2\right)-\Gamma k\omega\cos(k_x)+2\right) \\ \frac{1}{2}\omega\left(A\Gamma\left(3\phi_0^2-1\right)-\Gamma k\cos(k_x)+\Gamma k+(u_x-1)u_x\right) \end{pmatrix} \qquad \text{(A.3)}$$
$$A_3 = \begin{pmatrix} \omega\left(\gamma\left(-3A\phi_0^2+A-k\right)+\Gamma k\cos(k_x)-u_x^2+1\right) \\ \frac{1}{2}\omega\left(A\Gamma\left(3\phi_0^2-1\right)-\Gamma k\cos(k_x)+\Gamma k+u_x^2+u_x\right) \\ \frac{1}{2}\left(\omega\left(\Gamma\left(3A\phi_0^2-A+k\right)+(u_x-2)(u_x+1)\right)-\Gamma k\omega\cos(k_x)+2\right) \end{pmatrix}$$

## Appendix B.

The Miller theorem 6.1 [44] sequentially reduces the degree of the characteristic polynomial keeping the von Neumann stability of the initial polynomial. This was successfully applied to obtain the diffusion-dominant constraints for the linear TRT schemes [29] with DdQ(2d+1), D2Q9 and $D3Q15$ velocity sets and to construct exact advection-diffusion stability boundaries for the D1Q3 model [37]. Similarly, we build the third order characteristic equation for the phase equation and apply twice the Miller's polynomial reducing to obtain the linear equation with respect to amplification factor $\Omega$:

$$|\Omega|^2 = \frac{(d+eu_x^2+fu_x^4)^2+(k+lu_x^2)^2u_x^2}{(a+bu_x^2+cu_x^4)^2}, \qquad \text{(B.1)}$$

where, with $m = \tan\left(\frac{k_x}{2}\right)$:

$$
\begin{aligned}
a =& \Big(m^4\big(-\big(4A\Gamma(\omega-1)+8\Gamma k(\omega-1)+(\omega-2)^2\big)\big)-2m^2(2A\Gamma(\omega-1)+(\omega-2)\omega+2)-\omega^2\Big)\\
&\Big(m^4\big(-4\Gamma\omega(A+2k)+4\Gamma(A+2k)+\omega^2\big)+2m^2(-2A\Gamma(\omega-1)+(\omega-2)\omega+2)+(\omega-2)^2\Big)\\
b =& 4m^2\left(m^2+1\right)(\omega-1)^2\left(m^4(4a\Gamma+8\Gamma k-2)+m^2(4A\Gamma+1)+3\right)\\
c =& 4m^4(1+m^2)^2(-1+\omega)^2\\
d =& \Big(m^4\big(4A\Gamma(\omega-1)+8\Gamma k(\omega-1)+(\omega-2)^2\big)+2m^2(2A\Gamma(\omega-1)+(\omega-2)\omega+2)+\omega^2\Big)\\
&\Big(m^4\big(4A\Gamma((\omega-1)\omega+1)+8\Gamma k((\omega-1)\omega+1)-\omega^2\big)+m^2\big(4A\Gamma((\omega-1)\omega+1)\\
&-2((\omega-2)\omega+2)\big)-(\omega-2)^2\Big)\\
e =& 2m^2\Big(m^6(8A\Gamma(\omega-1)((\omega-1)\omega+1)+16\Gamma k(\omega-1)((\omega-1)\omega+1)+(\omega-4)\omega((\omega-2)\omega+2)+4)\\
&+m^4(16A\Gamma(\omega-1)((\omega-1)\omega+1)+16\Gamma k(\omega-1)((\omega-1)\omega+1)+\omega(\omega(\omega(3\omega-16)+30)\\
&-28)+14)+m^2(8A\Gamma(\omega-1)((\omega-1)\omega+1)+((\omega-2)\omega+2)(\omega(3\omega-8)+8))\\
&+(\omega-2)\omega((\omega-2)\omega+6)+6\Big)\\
f =& 4m^4\left(m^2+1\right)^2(\omega-1)((\omega-1)\omega+1)\\
k =& -2m\big(m^2+1\big)\Big(8A\Gamma\big(m^2+1\big)m^2(\omega-1)((\omega-1)\omega+1)+16\Gamma k m^4(\omega-1)((\omega-1)\omega+1)\\
&-\big(m^2+1\big)\omega^2\big(\omega\left(m^2\omega+\omega-4\right)+4\big)\Big)\\
l =& -8m^3\left(m^2+1\right)^2(\omega-1)((\omega-1)\omega+1)
\end{aligned}
\tag{B.2}
$$

## References

1. B. Ahrenholz, J. Tölke, P. Lehmann, A. Peters, M. Krafczyk, and W. Durner. Prediction of capillary hysteresis in a porous material using lattice-Boltzmann methods and comparison to experimental data and a morhphological pore network model. 31(9):1151–1173, 2008.
2. S. Bogner and U. Rude. Simulation of floating bodies with the lattice Boltzmann method. *Comp. Math. Appl.*, 65:901–913, 2013.
3. M. Bouzidi, M. Firdaouss, and P. Lallemand. Momentum transfer of a Boltzmann-lattice fluid with boundaries. *Phys. Fluids*, 13:3452–3459, 2001.
4. A.J. Briant, A.J. Wagner, and J.M. Yeomans. Lattice Boltzmann simulations of contact line motion. I. Liquid-gas systems. *Phys. Rev. E*, 69(031602):1–14, 2004.
5. C. Chena, L. Zenga, and L. Shid. Continuum-scale convective mixing in geological co2 sequestration in anisotropic and heterogeneous saline aquifers. *Adv. Water Res.*, 58(175187), 2013.

6. B. Chun and A.J.C. Ladd. Interpolated boundary condition for lattice Botlzmann simulations of flows in narrow gaps. *Phys. Rev. E*, 75(066705):1–12, 2007.
7. P.J. Dellar. Nonhydrodynamic modes and a priori construction of shallow water lattice Boltzmann equations. *Phys. Rev. E*, 65(036309):1–12, 2002.
8. P.J. Dellar. Lattice Kinetic Formulation for Ferrofluids. *J. Stat. Phys.*, 121: 105–118, 2005.
9. D. d'Humières. Generalized Lattice-Boltzmann Equations. *Rarefied Gas Dynamics: Theory and Simulations. Prog. Astronaut. Aeronaut.*, 159:450–458, 1992.
10. D. d'Humieres and I. Ginzburg. Viscosity independent numerical errors for Lattice Botlzmann models: From recurrence equations to "magic" collision numbers. *Comp. Math. Appl.*, 58(5):823–840, 2009.
11. D. d'Humières, I. Ginzburg, M. Krafczyk, P. Lallemand, and L.-S. Luo. Multiple-relaxation-time lattice Boltzmann models in three dimensions. *Phil. Trans. R. Soc. Lond. A*, 360:437–451, 2002.
12. U. D'Ortona, D. Salin, M. Cieplak, R.B. Rybka, and J.R. Banavar. Two-color nonlinear Boltzmann cellular automata: Surface tension and wetting. *Phys. Rev. E*, 51:3718, 1995.
13. F. Dubois and P. Lallemand. Towards higher order lattice Boltzmann schemes. *J. Stat. Mech.: Theory and Exp.*, P06(P06006), 2009.
14. M.M. Dupin, I. Halliday, and C.M. Care. Multi-component lattice Boltzmann equation for mesoscale blood flow. *J. Phys. A: Math. Gen.*, 36:8517–8534, 2003.
15. Ferréol and D. Rothman. Lattice-Boltzmann simulations of flow through Fointainebleau sandstone. *Transp. Porous Media*, 20(3), 1995.
16. U. Frisch, D. d'Humieres, B. Hasslacher, P. Lallemand, Y. Pomeau, and J.-P. Rivet. Lattice gas hydrodynamics in two and three dimensions. *Complex Systems*, 1:649–707, 1987.
17. A. Genty and V. Pot. Numerical Simulation of 3d Liquid-Gas Distribution in Porous Media by a Two-Phase trt Lattice Boltzmann Method. *Transp. Porous Media*, 96:271–294, 2013.
18. I. Ginzbourg and P.M Adler. Surface Tension Models with Different Viscosities. *Transp. Porous Media*, 20:37–76, 1995.
19. I. Ginzbourg and D. d'Humiéres. Local Second-Order Boundary method for Lattice Boltzmann models. *J. Stat. Phys.*, 84(5/6):927–971, 1996.
20. I. Ginzburg. Variably saturated flow described with the anisotropic Lattice Boltzmann methods. *Comput. Fluids*, 35:831–848, 2006.
21. I. Ginzburg. Lattice Boltzmann modeling with discontinious collision components: Hydrodynamic and Advection-Diffusion Equations. *J. Stat. Phys.*, 126 (1):157–206, 2007.
22. I. Ginzburg. Consistent Lattice Boltzmann schemes for the Brinkman model of porous flow and infinite Chapman-Enskog expansion. *Phys. Rev. E*, 77(066704): 1–12, 2008.
23. I. Ginzburg. Truncation errors, exact and heuristic stability analysis of two-

relaxation-times lattice boltzmann for anisotropic advection-diffusion equation schemes. *Commun. Comput. Phys.*, 5(11):1439–1502, 2012.

24. I. Ginzburg. Multiple anisotropic collisions for advection-diffusion Lattice Boltzmann schemes. *Adv. Water Res.*, 51:381–404, 2013.
25. I. Ginzburg and D. d'Humières. Multireflection boundary conditions for lattice Boltzmann models. *Phys. Rev. E*, 68(066614):1–30, 2003.
26. I. Ginzburg and K. Steiner. A free-surface lattice Boltzmann method for modelling the filling of expanding cavities by Bingham fluids. *Phil. Trans. R. Soc. Lond. A*, 360:453–466, 2002.
27. I. Ginzburg, F. Verhaeghe, and D. d'Humières. Two-relaxation-time Lattice Boltzmann scheme: about parametrization, velocity, pressure and mixed boundary conditions. *Commun. Comput. Phys.*, 3(2):427–478, 2008.
28. I. Ginzburg, F. Verhaeghe, and D. d'Humières. Study of Simple Hydrodynamic Solutions with the Two-Relaxation-Times Lattice Bolzmann Scheme. *Commun. Comput. Phys.*, 3(3):519–581, 2008.
29. I. Ginzburg, D. D'Humieres, and A. Kuzmin. Optimal Stability of Advection-Diffusion Lattice Boltzmann Models with Two Relaxation Times for Positive/Negative Equilibrium. *J. Stat. Phys.*, 139(6):1090–1143, 2009.
30. A.K. Gunstensen, D.H. Rothman, S. Zaleski, and G. Zanetti. Lattice Boltzmann model of immiscible fluids. *Phys. Rev. A*, 43(8):4320–4327, 1991.
31. H. Hammou, I. Ginzburg, and M. Boulerhcha. Two-relaxation-times lattice boltzmann schemes for solute transport in unsaturated water flow, with a focus on stability. *Adv. Wat. Res.*, 34(6):779–793, 2011.
32. F.J. Higuera and J. Jimenez. Boltzmann Approach to Lattice Gas Simulations. *Europhys. Lett.*, 9(7):663–668, 1989.
33. F.J. Higuera, S. Succi, and R. Benzi. Lattice gas dynamics with enhanced collisions. *Europhys. Lett.*, 9(4):345–349, 1989.
34. D. Kehrwald. *Numerical Analysis of Immiscible Lattice BGK*. PhD thesis, Fraunhofer-Institut für Techno- und Wirtschaftsmathematik, 2002.
35. V.M. Kendon, M.E. Cates, I. Pagonabarraga, J.-C. Desplat, and P. Bladon. Inertial effects in three-dimensional spinoidal decomposition of a symmetric binary fluid mixture: a lattice Boltzmann study. *J. Fluid Mech.*, 440:147–203, 2001.
36. A.E. Komrakova, D. Eskin, and J.J. Derksen. Lattice Boltzmann simulations of a single n-butanol drop rising in water. *Phys. Fluids*, 25(042102):1–29, 2013.
37. A. Kuzmin, I. Ginzburg, and A.A. Mohamad. The role of the kinetic parameter in the stability of two-relaxation-time advection-diffusion lattice Boltzmann schemes. *Comp. Math. Appl.*, 61:3417–3442, 2011.
38. A. Kuzmin, M. Januszewski, D. Eskin, F. Mostowfi, and J. Derksen. Simulations of gravity-driven flow of binary liquids in microchannels. *Chem. Eng. J.*, 171 (2):646–654, 2011.
39. A. Kuzmin, M. Januszewski, D. Eskin, F. Mostowfi, and J. Derksen. Three-dimensional binary-liquid lattice boltzmann simulation of microchannels with

rectangular cross sections. *Chem. Eng. J.*, 178:306–316, 2011.

40. P. Lallemand and L.-S. Luo. Theory of the lattice Boltzmann method: Dispersion, dissipation, isotropy, Galilean invariance, and stability. *Phys. Rev. E*, 61 (6):6546–6562, 2000.
41. M. Latva-Kokko and D.H. Rothman. Diffusion properties of gradient-based lattice Boltzmann models of immiscible fluids. *Phys. Rev. E*, 71(056702):1–8, 2005.
42. H. Liu, J.G. Zhou, M. Li, and Y. Zhao. Multi-block lattice Boltzmann simulations of solute transport in shallow water flows. *Adv. Water Res.*, 58:24–40, 2013.
43. W. Long, H. Huang, J. Serlemitsos, E. Liu, A.H. Red, and M. Hilpert. Porescale study of the collector efficiency of nanoparticles in packings of nonspherical collectors. *Coll. Surf. A: Physicochem. Eng. Aspects*, 358:163–171, 2010.
44. J.J.H. Miller. On the Location of Zeros of Certain Classes of Polynomials with Applications to Numerical Analysis. *J. Inst. Maths Applics*, 8:397–406, 1971.
45. I. Pagonabarraga, A.J. Wagner, and M.E. Cates. Binary Fluid Demixing: The Crossover Region. *J. Stat. Phys.*, 107:39–52, 2002.
46. Y. Peng, J.G. Zhou, J.M. Zhang, and R. Burrows. Modelling moving boundary in shallow water by lbm. *Int. J. Mod. Phys. C.*, 24(1250094), 2013.
47. C.M. Pooley, H. Kusumaatmaja, and J.M. Yeomans. Contact line dynamics in binary lattice Boltzmann simulations. *Phys. Rev. E*, 78(056709):1–9, 2008.
48. C.M. Pooley, H. Kusumaatmaja, and J.M. Yeomans. Modeling capillary filling dynamics using lattice Boltzmann simulations. *Eur. Phys. J. Special Topics*, 171:63–71, 2009.
49. K.N. Premnath and J. Abraham. Simulations of binary drop collisions with a multiple-relaxation-time lattice-Boltzmann model. *Phys. Fluids*, 17(122105): 1–21, 2005.
50. Y.H. Qian, D. d'Humières, and P. Lallemand. Lattice BGK Models for Navier-Stokes Equation. *Europhys. Lett.*, 17(6):479–484, 1992.
51. T. Reis and P.J. Dellar. A volume-preserving sharpening approach for the propagation of sharp phase boundaries in multiphase Boltzmann simulations. *Comput. Fluids*, 46:417–421, 2011.
52. T. Reis and T.N. Philips. An Alternative Approach to the Solution of the Dispersion Relation for a Generalized Lattice Boltzmann Equation. *Phys. Rev. E*, 77(026702), 2008.
53. B. Servan-Camas and F. T.-C. Tsai. Lattice Boltzmann method with two relaxation times for advection-diffusion equation: Third order analysis and stability analysis. *Adv. Wat. Res.*, 31:1113–1126, 2008.
54. B. Servan-Camas and F. T.-C. Tsai. Saltwater intrusion modeling in heterogeneous confined aquifers using two-relaxation-time Lattice Boltzmann method. *J. Comp. Phys.*, 228:236–256, 2009.
55. B. Servan-Camas and F. T.-C. Tsai. Non-negativity and stability analyses of lattice boltzmann method for advection-diffusion equation. *J. Comput. Phys.*,

228:236–256, 2009.

56. X. Shan. Analysis and reduction of the spurious current in a class of multiphase lattice Boltzmann models. *Phys. Rev. E*, 73(047701):1–4, 2006.
57. X. Shan and H. Chen. Simulation of nonideal gases and gas-liquid phase transitions by the lattice Boltzmann Equation. *Phys. Rev. E*, 49(4):2941–2948, 1994.
58. M.R. Swift, W.R. Osborn, and J.M. Yeomans. Lattice Boltzmann Simulation of Nonideal Fluids. *Phys. Rev. Lett.*, 75(5):831–834, 1995.
59. L. Talon, D. Bauer, N. Gland, H. Auradou, and I. Ginzburg. Assessment of the Two Relaxation Time Lattice Boltzmann scheme to simulate Stokes flow in porous media. *Wat. Res. Res.*, 48(W04526):1–13, 2012.
60. M. Thies. *Lattice Boltzmann Modelling with Free Surfaces Applied to In-situ Gas Generated Foam Formation*. PhD thesis, Erlangen, 2005.
61. J. Thömmes, J. Becker, M. Junk, A.K. Vaikuntam, D. Kerhwald, A. Klar, K. Steiner, and A. Wiegmann. A Lattice Boltzmann Method for immiscible multiphase flow simulations using the Level Set Method. Technical report, Fraunhofer-Institut für Techno- und Wirtschaftsmathematik ITWM, 2007.
62. J. Tölke, G. De Prisco, and Y. Mu. A lattice Boltzmann method for immiscible two-phase Stokes flow with a local collision operator. *Comp. Math. Appl.*, 65 (6):864–881, 2013.
63. A. Vikhansky. Lattice-Boltzmann method for yield-stress liquids. *J. Non-Newtonian Flud Mehc.*, 155:95–100, 2008.
64. S.D.C. Walsh and M.O. Saar. Macroscale lattice-Boltzmann methods for low Peclet number solute and transport in heterogeneous porous media. *Water Res. Res.*, 46:1–15, 2010.
65. Wolfram. Mathematica, 2011.
66. J. Yang and E.S. Boek. A comparison study of multi-component Lattice Boltzmann models for flow in porous media applications. *Comp. Math. Appl.*, 65(6): 882–890, 2013.
67. P. Yuan and L. Schaefer. A Thermal Lattice Boltzmann Two-Phase Flow Model and Its Application to Heat Transfer Problems -Part 2. Integration and Validation. *J. Fluids Eng.*, 128:151–156, 2006.
68. H.W Zheng, C. Shu, and Y.T. Chew. A lattice Boltzmann model for multiphase flows with large density ratio. *J. Comput. Phys.*, 218:353–371, 2006.